

Spin-Polarized Electron Transport through Nanometer-Scale Al Grains

L. Y. Zhang, C. Y. Wang, Y. G. Wei, X. Y. Liu, and D. Davidović

Georgia Institute of Technology, Atlanta, GA 30332

(Dated: November 5, 2018)

We investigate spin-polarized electron tunnelling through ensembles of nanometer scale Al grains embedded between two Co-reservoirs at 4.2K, and observe tunnelling-magnetoresistance (TMR) and effects from spin-precession in the perpendicular applied magnetic field (the Hanle effect). The spin-coherence time (T_2^*) measured using the Hanle effect is of order ns . The dephasing is attributed to electron spin-precession in local magnetic fields. Dephasing process does not destroy *TMR*, which is strongly asymmetric with bias voltage. The asymmetric TMR is explained by spin relaxation in Al grains and asymmetric electron dwell times.

Long spin relaxation times for polarized carriers are necessary for development of spintronic devices. In quantum dots, spin relaxation times are strongly enhanced compared to bulk, and the spin of an electron confined in a quantum dot is a candidate quantum bit [1, 2]. Unfortunately, the spin-coherence time T_2^* measured in a semiconducting quantum dot is only $\sim ns$, [3] despite the fact that the spin-relaxation time (T_1) is extremely long, up to a $\sim ms$ [4, 5]. In GaAs quantum dots, dephasing is caused by spin precession around an effective magnetic field created by nuclear spins.

Spin-injection and detection from ferromagnetic electron reservoirs is a well-known technique to measure spin relaxation time [6]. In this paper we study electron spin-injection in tunnelling junctions containing a large number of embedded Al-grains.

Our tunnelling device is sketched in Fig. 1-A. The top and the bottom layers are 100Å thick Co films. The width/length is 1.5mm/15mm and 1mm/20mm for the bottom and the top layer, respectively. The sample cross-section, sketched in Fig. 1-B, shows nanometer scale Al grains embedded in aluminum oxide. The device is a recreation of a tunnelling device made by Zeller and Giaver in the 1960s [7], which demonstrated Coulomb Blockade for the first time. The difference between our sample and the prior devices is that we have spin-polarized leads.

The device is fabricated in two evaporation steps. First, we thermally evaporate a Co film on a SiO_2 substrate, through a mask at $4 \cdot 10^{-7}$ Torr pressure. The

deposition of cobalt is stopped by closing the shutter. Next, we change the metal source to Al and evaporate Aluminum in high vacuum, while the shutter remains closed. Then we open the shutter for 1 second and close the shutter again. The deposition rate is 0.2nm/sec. So, Co layer is now covered with a seed layer of Al with nominal thickness 0.2nm.

Our next deposition step is reactive deposition of aluminum oxide. In this step, oxygen is introduced into the chamber, which exposes the cobalt surface to oxygen vapor. The oxidation of Cobalt surface should be minimal, because paramagnetic impurities in cobalt-oxide could affect spin-polarized tunnelling. Our strategy to minimize oxidation of Co is to apply as little oxygen as possible for as little time as possible. In addition, the seed layer also provides some protection of Co before passivation by the deposited aluminum oxide. The seed layer must be very thin, because if any metallic Al remains on Co surface after oxidation, then spin-polarized tunnelling density of states will be reduced.

Immediately after closing the shutter the second time, we introduce oxygen into the deposition chamber while evaporating Al. The oxygen is introduced at a flow rate of 200 sccm. The chamber is continuously pumped with the cryopump gate valve fully open. Oxygen pressure increases and reaches 10^{-5} scale Torr in few seconds and stabilizes at $3 \cdot 10^{-5}$ Torr after 30 sec. Only during these initial 30 seconds, while the pressure increases and stabilizes, cobalt surface with a 0.2nm seed layer of Al is exposed to oxygen. After 30 sec, when the pressure is stabilized, we open the shutter and evaporate 5nm of Al at a rate of 0.2nm/s, to deposit the bottom aluminum-oxide film, which is 7nm thick.

In general, the thickness of the deposited oxide at fixed aluminum evaporation rate will be an increasing function of oxygen pressure. In our case, thickness of the deposited oxide versus pressure saturates at 7nm at approximately $1 \cdot 10^{-5}$ Torr. Any further increase in oxygen pressure will not increase the aluminum oxide thickness. Consequently, in our deposition process nearly all Al atoms that are deposited at $3 \cdot 10^{-5}$ Torr are oxidized, however, the oxygen pressure is only three times larger than the minimal oxygen pressure for the oxidation of Al

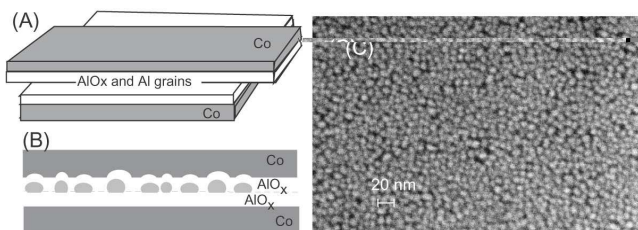


FIG. 1: A: Sketch of the tunnelling device geometry. B: Sketch of the tunnelling junction cross-section. C: Scanning electron micrograph of Al grains.

(the saturation pressure).

The oxygen pressure of $3 \cdot 10^{-5}$ is substantially smaller than typical oxygen pressures used to thermally oxidize Al surfaces in tunnelling junctions. For example, in Ref. [8], nanometer sized Al nanoparticles were oxidized at 0.1 Torr of oxygen for 1-2 minutes. This process created tunnelling barriers of resistance in $M\Omega$ range, which corresponds to oxide thickness of approximately 1nm. Since our oxygen pressure is smaller by four orders of magnitude and the oxidation time is shorter, the thickness of the surface aluminum oxide in our case must be considerably smaller than 1nm. Thus, we expect that the seed Al-layer of nominal thickness 0.2nm provides some protection of Co surface from oxidation.

Prior to this work, this reactive evaporation technique was used to create tunnelling junctions containing a single metallic grain. [9] The junctions were of high quality and they displayed well resolved Coulomb-Blockade steps and discrete energy levels of the grain at low temperatures. So, the aluminum oxide in our samples is a suitable insulator for the studies of properties of metallic grains.

The sample, which is now passivated, is exposed to air and the mask is replaced. Next, the sample is evacuated to base pressure and we deposit 1.5 nm of Al, which creates isolated grains, as shown by the image in Fig. 1-C. Then we deposit another layer of aluminum oxide, by evaporating 5nm of Al at rate 0.2nm/s at $3 \cdot 10^{-5}$ Torr of oxygen. Finally, we deposit the top Co layer.

The average grain diameter is $\sim 6nm$. If we assume that the grains are hemispherical, analogous to Ref. [8], we estimate that the average electron-in-a-box mean level spacing is $0.2meV$. Note that there is a relatively wide distribution of grain diameters in Fig. 1-C, as some grains have coalesced. Hence, the range of level spacings in the ensemble is rather large.

In addition, the grains are exposed to oxygen vapor before deposition of the top oxide layer, at $3 \cdot 10^{-5}$ Torr for 30 seconds. As a result, the grain surface is oxidized from above, but we expect that the oxide thickness is considerably smaller than 1nm, as discussed above. Additionally, there is generally chemisorbed oxygen remaining on the underlying oxide surface. Consequently, the grain surface may be oxidized from below. Thus, the average size of the metallic core of the grains could be smaller than the apparent grain size because of this effect, by up to about 1 nm.

The number of grains in the junctions is $N = 2.5 \cdot 10^{10}$. Although the junctions are very large, the resistance of the junctions (R) varies significantly among samples made at the same time. R is in the range $1k\Omega < R < 1M\Omega$. We also make tunnelling junctions as described above but without Al grains and find these devices to be insulating. In addition, we make control samples without Al grains and with the aluminum-oxide layers at half the thicknesses from those above. The control sample resistance is in the same range ($1k\Omega < R < 1M\Omega$),

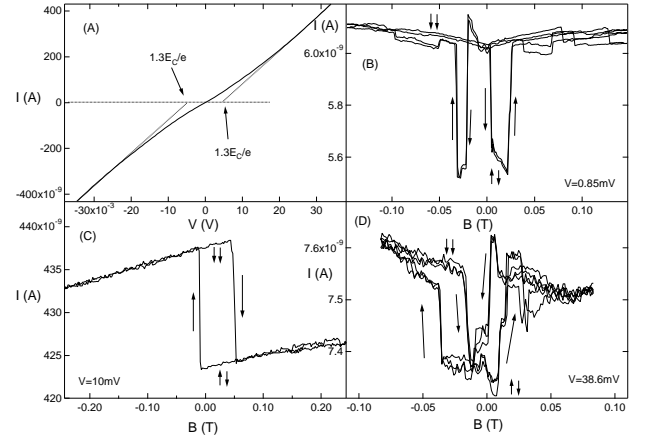


FIG. 2: A: IV-curves of sample 1 at 4.2K. B, C, and D: Current versus parallel applied magnetic field at 4.2K, in samples 1, 2, and 3, respectively.

which shows that tunnelling in the devices with grains take place via the grains.

The fluctuations in sample resistance among samples made at the same time show that the tunnel current must be dominated by the current flow through weak spots. Consequently, the number of grains that are active in transport is $\ll N$. The weak spots may result from thickness variations in the oxide layer across the junction area or from defects in the oxide, or from both.

We measured the surface roughness of a single aluminum oxide film deposited over SiO_2 by the atomic-force microscope and found that it was $\approx nm$. This surface roughness can cause weak spots in the tunnelling barrier, because the tunnel resistance decay length in oxides ($0.1nm$) is much smaller than the surface roughness.

In addition, it is known that amorphous aluminum oxide has coordination number defects, which may be caused by oxygen vacancies. [10] These defects could give rise to hole traps near the valence band edge, which could result in weak spots for tunnelling. These oxygen vacancies could be paramagnetic, which could affect spin-polarized tunnelling.

In this paper we present three devices with Al grains. Fig. 2-A displays the IV-curve of sample 1 at 4.2K. The other two samples have similar IV-curves. The conductance is suppressed at zero bias voltage, as expected from Coulomb-Blockade on Al-grains, consistent with Ref. [7].

The average charging energy E_C is obtained by extrapolating the linear part of the IV-curve at high V to zero I and finding the offset voltage, as indicated. We averaged the Coulomb Staircase IV-curve [11] over the background charge, capacitance ratios, and over capacitance range ($C/4, 7C/4$), where C is the total capacitance of a grain. The corresponding offset was $1.3E_C/e$, where $E_C = e^2/2C$. E_C is $4.3meV$ in samples 1 and 2 and $6meV$ in sample 3.

Figs. 2-B,C, and D display current versus magnetic field in samples 1,2, and 3 respectively, at constant bias voltage. All samples exhibit *TMR*, which demonstrates that the tunnelling current is spin-polarized. Samples 1 and 3 exhibit a spin-valve effect: at a large negative field, the magnetizations of the Cobalt reservoirs are down. If the field increases, the magnetization of one Cobalt reservoir switches direction, and the tunnelling current drops abruptly from $I_{\downarrow\downarrow}$ to $I_{\uparrow\downarrow}$. Finally, at a larger positive field the current jumps back up to $I_{\uparrow\uparrow} \approx I_{\downarrow\downarrow}$.

In addition to these abrupt transitions in *TMR*, we find that *TMR* varies continuously with the magnetic field and it fully saturates in the applied field of $\sim 1T$. Co-films are generally multi-domain, and the average domain size in Co films is of the order of 1 micron. [12] If many domains were involved in providing the *TMR* signal, one would expect the resistance transitions to be gradual due to the spread in coercive fields from domain to domain. Thus, only a portion of the sample of order domain size or less is responsible for the abrupt *TMR* transitions. This behavior is in agreement with the finding that the tunnelling current is dominated by weak spots.

In sample 2, there is only one jump near zero field, followed by a broad *TMR* background that saturates at $B \sim 1T$, which shows that only one cobalt electrode exhibits an abrupt transition with magnetic field. The abruptness of the transition indicates again that this sample is sensitive to a very small fraction of the physical device. However, in contrasts to samples 1 and 3, the magnetic behavior of Co on one side of the effective contact area indicates the presence of a very persistent magnetic defect, which could be for example a 360 degree domain wall. [13]

Although our junctions are not ideal, we can learn about the physics of spin-polarized tunnelling through grains by studying how the abrupt resistance transitions depend on bias voltage and the perpendicular applied magnetic field. *TMR* corresponding to these transitions is a measure of the spin-polarization of the current. The number of particles that contribute to the abrupt transitions is very small. It is certainly smaller than the number of particles that fit under a micron scale domain in Cobalt (roughly 10^4). The abrupt *TMR* transitions are reproducible when the magnetic field cycle is repeated, as seen in Fig. 2. For the Hanle effect studies, we select devices that exhibit spin-valve effect.

The tunnelling magnetoresistance is calculated as

$$TMR = (I_{\uparrow\uparrow} - I_{\uparrow\downarrow})/I_{\uparrow\downarrow}, \quad (1)$$

where the current values were taken immediately before and after the resistance transitions. Figs. 3-A and B display differential conductance G with bias voltage in samples 1 and 2, respectively. G is measured by the lock-in technique. As the bias voltage is varied slowly at 3mv/hr, the magnetic field is swept between -0.25T and 0.25T at 0.01Hz. The differential conductance switches

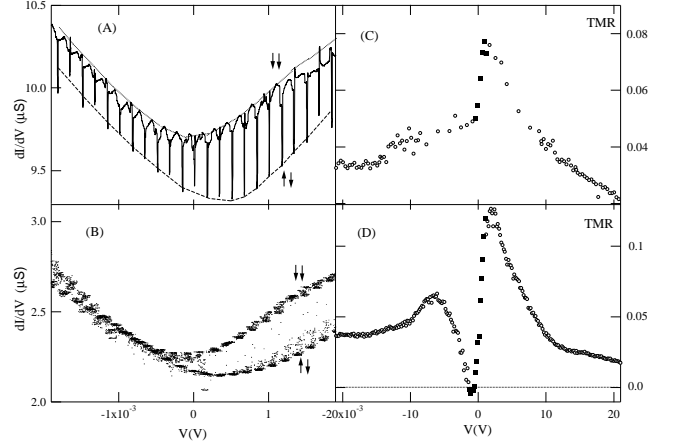


FIG. 3: A and B: Differential conductance versus bias voltage in samples 1 and 2, respectively. C and D: *TMR* versus bias voltage in samples 1 and 2, respectively.

between $G_{\uparrow\uparrow}$ and $G_{\uparrow\downarrow}$ when the magnetizations switch alignment.

$G_{\uparrow\uparrow} - G_{\uparrow\downarrow}$ changes significantly when the bias voltage varies in a narrow interval around zero-bias voltage. In sample 2, the asymmetry in $G_{\uparrow\uparrow} - G_{\uparrow\downarrow}$ is dramatic: conductance is spin-unpolarized at negative bias and significantly spin-polarized at positive bias. *TMR* also changes significantly around zero bias voltage, as shown in Fig. 3-C and D. Circles represent *TMR* from Eq. 1, and squares are obtained as $TMR = \int G_{\uparrow\uparrow}(V)dV / \int G_{\uparrow\downarrow}(V)dV - 1$.

TMR values in our devices are less than 10%. In state of the art magnetic tunnelling junctions, *TMR* exceeds 40% at room temperature and it is critically dependent upon the fabrication process and annealing of the tunnelling junctions. [14] As discussed before, tunnelling in our samples is dominated by weak spots caused by the surface roughness and oxygen vacancies. The junctions are not ideal and thus the *TMR* is reduced.

In non-ideal magnetic tunnelling junctions, *TMR* can be strongly asymmetric and bias voltage dependent. [15, 16, 17, 18] The asymmetry has been explained by the two-step tunnelling via localized states. In our control samples (without grains), *TMR* is found to be symmetric and weakly dependent on V . This shows that the localized states responsible for asymmetric *TMR* in junctions with grains are the electronic states in the grains.

We explain the asymmetry in *TMR* by spin-relaxation in Al grains and the asymmetry between the resistance between the grains and the two reservoirs. Asymmetric resistances are easily introduced by sample fabrication. For example, exposure of the bottom aluminum oxide layer to air increases the oxide thickness by hydration.

The average dwell time is $\tau_D \sim \frac{R_D}{R_Q} \frac{h}{\delta}$, where R_D is the average resistance between the grains and the drain reservoir, and $R_Q = 26k\Omega$. When the bias voltage changes sign, the drain reservoir changes, so τ_D also changes.

Asymmetric *TMR* occurs when the spin-relaxation time T_1 is smaller than the longer dwell time. For example, in sample 2, figure 3-B suggests that T_1 is much smaller than the dwell time at negative bias, and T_1 is comparable to or longer than the dwell time at positive bias. The voltage interval around zero bias where the dwell times change is given by the Coulomb Blockade thermal width $7k_B T/e$, in agreement with Fig. 3.

At large magnitude of bias voltage, *TMR* has a complex dependence on the magnitude of bias voltage. It is difficult to explain the origin of this dependence, but we speculate that energy dependence of the spin relaxation time, single electron charging effects, and the distribution of energy level spacings in the ensemble of grains may play important roles.

Next, we discuss the effects of spin precession in the applied magnetic field (the Hanle effect). We measure current versus magnetic field B_n applied perpendicular to the film. Fig. 4-A displays the resulting peak in current versus B_n , for sample 3 in the antiparallel configuration (in zero applied parallel field). The dependence is reversible when B_n is swept up and down, which shows that the curve does not arise from the hysteresis loop in the leads. The peak amplitude is $(I_{\uparrow\uparrow} - I_{\uparrow\downarrow})/2$.

The characteristic field B_C , defined as half-width of the peak, is 8mT. We find that B_C is symmetric with bias voltage, which shows that B_C is independent of the dwell time. So, the processes that contribute to the Hanle effect half-width are different from the processes responsible for the *TMR*-asymmetry. We have confirmed the Hanle effect in one more sample, however the half-width was $2mT$.

The Hanle effect in a quantum dot has recently been calculated by Braun et al. [?] The calculation shows that perpendicular field induces Larmor precession of the injected spin, which reduces spin polarization of the current. Current versus B_n exhibits a Lorentzian peak of amplitude $(I_{\uparrow\uparrow} - I_{\uparrow\downarrow})/2$ (in agreement with our data) centered at $B_n = 0$. If a constant large parallel magnetic field B^* is present, then the peak width becomes B^* and the Hanle effect half-width is symmetric with bias voltage.

Our observations (Fig. 4-A) can be explained by these theoretical results, if in zero applied field there exist a local magnetic field B_C acting on the grains. This local field induces spin precession in zero applied magnetic field, and the spin-coherence time is the Larmor period in the local field: $T_2^* \sim \hbar/\mu_B B^* \sim ns$.

The local field could be caused by the surface roughness, which generates a finite dipole field originating from Co. Note that the top aluminum-oxide/cobalt interface in Fig. 1-B is quite rough because of the underlying Aluminum grains. The local field of 8mT is certainly possible because the internal field in Co is 2T. The hyperfine field from the nuclei can also create an effective field of order mT that causes dephasing. [3] In our junctions,

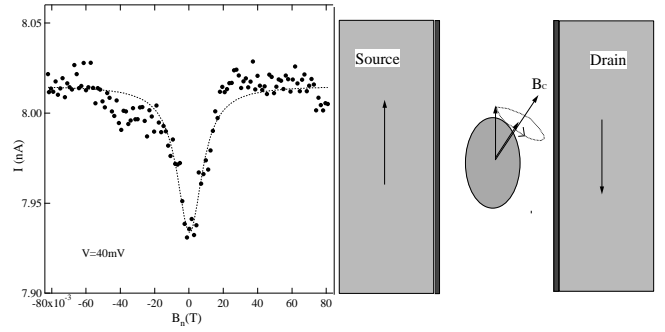


FIG. 4: A. Current versus perpendicular field in sample 3. B. Sketch of the effects of the local field on TMR. The component of the injected spin along the local field direction gives rise to a finite TMR, even if T_2^* is much shorter than the dwell time.

tunnelling is dominated by weak spots. Consequently, the local magnetic field will fluctuate among samples, explaining the difference in B_C between the samples.

TMR survives dephasing because of the conservation of spin-component along the local field direction. Even if the electron dwell time is much longer than the dephasing time, *TMR* will be finite. This is sketched in Fig. 4-B. If the magnetizations switch from parallel to antiparallel state at finite V , then the injected spin component along the local field direction switch from zero to finite value, giving rise to a finite TMR. The perpendicular component of the injected spin is averaged to zero, which reduces the TMR.

In conclusion, we study spin-polarized current through ensembles of nm-scale Al grains. The spin-coherence time is obtained from the Hanle effect measurement: $T_2^* \sim ns$. Fast dephasing is attributed to spin-precession in the local magnetic field. Tunnelling magnetoresistance is asymmetric with current direction, which we attribute to the asymmetry in electron dwell times and spin-relaxation. This work was performed in part at the Georgia-Tech electron microscopy facility. This research is supported by the David and Lucile Packard Foundation grant 2000-13874 and Nanoscience/Nanoengineering Research Program at Georgia-Tech.

-
- [1] D. Loss and D. P. DiVincenzo, Phys. Rev. A **57**, 120 (1998).
 - [2] G. Burkard, H. A. Engel, and D. Loss, Fortschr. Phys. **48**, 965 (2000).
 - [3] A. C. Johnson, J. R. Petta, J. M. Taylor, A. Yacoby, M. D. Lukin, C. M. Marcus, M. P. Hanson, and A. C. Gossard, Nature **435**, 925 (2005).
 - [4] T. Fujisawa, D. G. Austing, Y. Tokura, Y. Hirayama, and S. Tarucha, Nature **419**, 278 (2002).
 - [5] J. M. Elzerman, R. Hanson, L. H. W. van Beveren, B. Witkamp, L. M. K. Vandersypen, and L. P. Kouwen-

- hoven, *Nature* **430**, 6998 (2004).
- [6] M. Johnson and R. H. Silsbee, *Phys. Rev. Lett.* **55**, 1790 (1985).
 - [7] H. R. Zeller and I. Giaver, *Phys. Rev.* **181**, 789 (1969).
 - [8] D. C. Ralph, C. T. Black, and M. Tinkham, *Phys. Rev. Lett.* **74**, 3241 (1995).
 - [9] D. Davidović and M. Tinkham, *Phys. Rev. Lett.* **83**, 1644 (1999).
 - [10] Z. W. Zhao, B. K. Tay, C. Q. Sun, and V. Ligatchev, *Jour. Appl. Phys.* **95**, 4147 (2004).
 - [11] D. V. Averin and K. K. Likharev, in *Mesoscopic Phenomena in Solids*, edited by B. L. Altshuler, P. L. Lee, and R. A. Webb (Elsevier and Amsterdam, 1991), p. 169.
 - [12] J. Unguris, D. Tulchinsky, M. H. Kelley, J. A. Borchers, J. A. Dura, C. F. Majkrzak, S. Y. Hsu, R. Loloee, W. P. P. Jr., and J. Bass, *Journal of Applied Physics* **87**, 6639 (2000).
 - [13] A. Hubert and R. Schafer, *Domain Walls* (Springer-Verlag, 1998).
 - [14] S. S. P. Parkin, K. P. Roche, M. G. Samant, P. M. Rice, R. B. Beyers, R. E. Scheuerlein, E. J. O'Sullivan, S. L. Brown, J. Bucchigano, D. W. Abraham, et al., *Appl. Phys. Lett.* **75**, 301 (1999).
 - [15] J. Zhang and R. M. White, *Jour. Appl. Phys.* **83**, 6512 (1998).
 - [16] E. Y. Tsymbal, O. N. Mryasov, and P. R. LeClair, *Jour. Phys. Cond. Matt.* **15**, R109 (2003).
 - [17] E. Y. Tsymbal, A. Sokolov, I. F. Sabirianov, and B. Doudin, *Phys. Rev. Lett.* **90**, 186602 (2003).
 - [18] J. R. Petta, S. K. Slater, and D. C. Ralph, *Phys. Rev. Lett* **93**, 136601 (2004).